Progress In Electromagnetics Research, PIER 18, 127–150, 1998

MICROWAVE SPECIFIC ATTENUATION BY OBLATE SPHEROIDAL RAINDROPS: AN EXACT ANALYSIS OF TCS'S IN TERMS OF SPHEROIDAL WAVE FUNCTIONS

L. W. Li, T. S. Yeo, P. S. Kooi, and M. S. Leong

Communications & Microwave Division
Department of Electrical Engineering
National University of Singapore
10 Kent Ridge Crescent, Singapore 119260

1. INTRODUCTION

Scattering and attenuation of radio waves by raindrop scatterers have attracted many researchers worldwide over the past several decades. The most popular raindrop model for the analysis of rainfall attenuation in the published literature usually considers the raindrops as spheroidal raindrop scatterers. The methods and techniques employed for the analysis of specific rainfall attenuation are the boundary-perturbation and point-matching techniques by Oguchi [1, 2], the least-squares fitting process of boundary conditions by Morrison and Cross [3], the sphere-based Taylor expansion by Erma [4–6], the integral equation technique by Holt et al. [7], the T-matrix method by Waterman [8–10] and the method of extended boundary conditions by Warner [11, 12].

However, most of the above-mentioned methods are numerical-based approaches and cannot give an exact formulation of the scattered fields and the resultant total cross sections. To formulate exactly and calculate accurately the scattered fields by the dielectric spheroid and its total cross sections, the eigen-expansion method of spheroidal vector wave functions is a very good choice. This method was applied earlier by Asano and Yamamoto [13] who determined the expansion coefficients using the boundary conditions. However, since only the tabulated values given in the published work were used, Asano and Yamamoto presented the extinction cross sections which are valid only for the scattering from the lossless dielectric spheroid. Even with the modification made later by Asano & Yamamoto [13] and Cooray & Ciric [14], there is still no available extinction cross section data necessary for the calculation of rainfall attenuation.

In a similar fashion to the work by Asano and Yamamoto [13] , a *rigorous* formulation of the electromagnetic scattering from a *lossy* dielectric spheroid is given in this paper. The experimental data collected in the past show that the specific microwave attenuation due to rainfall in Singapore's tropic environment are much larger than those recommended by the CCIR (now known as ITU). With the exact expressions of the scattered fields and the extinction cross sections in terms of spheroidal vector wave eigenfunctions, the specific attenuation is integrated numerically by making use of the distribution of raindrop sizes in Singapore. The computed results are also compared with the experimental data collected in Singapore in the last three years and with the results previously published by Yeo et al. [15] and Li et al.

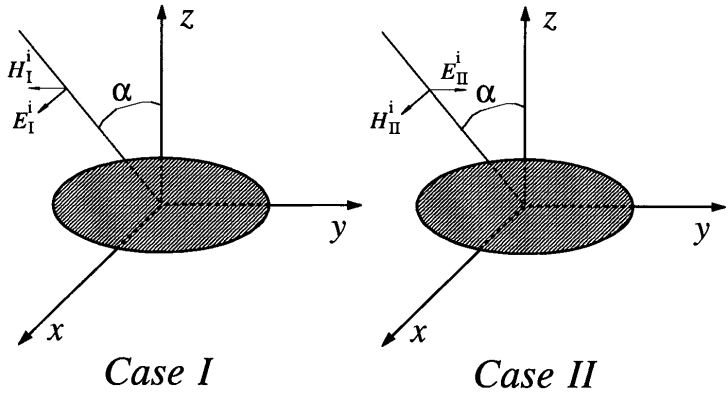

Figure 1. Geometry of electromagnetic scattering by oblate spheroidal raindrops.

[16–18]. Numerical techniques are also used in the data interpolation and an interpolated three-dimensional model of the extinction cross sections is established. With this model, the computational speed of the specific attenuation is increased significantly.

2. SPHEROIDAL COORDINATES

In this paper, an oblate spheroidal coordinates system is chosen. The oblate spheroidal coordinates are related to rectangular coordinates by the following transformation:

$$x = \frac{d}{2}\sqrt{(1-\eta^2)(\xi^2+1)}\cos\phi, \tag{1a}$$

$$y = \frac{d}{2}\sqrt{(1-\eta^2)(\xi^2+1)}\sin\phi, \tag{1b}$$

$$z = \frac{d}{2}\eta\xi, \tag{1c}$$

with

$$-1 \le \eta \le 1, \quad 0 \le \xi < \infty, \quad 0 \le \phi \le 2\pi, \tag{1d}$$

or

$$0 \le \eta \le 1, \quad -\infty < \xi < \infty, \quad 0 \le \phi \le 2\pi. \tag{1e}$$

The electromagnetic fields, $\mathbf{E}_f$ and $\mathbf{H}_f$ in the (outer and inner) f^{th} region (f =1 and 2) as shown in Fig. 1 are expressed by

$$\nabla \times \nabla \times \mathbf{E}_f - k_f^2 \mathbf{E}_f = 0, \tag{2a}$$

$$\nabla \times \nabla \times \mathbf{H}_f - k_f^2 \mathbf{H}_f = 0, \tag{2b}$$

where ϵ_f , μ_f and σ_f identify the permittivity, permeability and conductivity of the medium, respectively, and $k_f = \omega\sqrt{\mu_f \epsilon_f (1 + \frac{i\sigma_f}{\omega\epsilon_f})}$ is the propagation constant in the f^{th} layer of the multilayered medium. A time dependence $\exp(-i\omega t)$ is assumed to describe the electromagnetic fields throughout the paper. Moreover, the outside region I ($f = 1$) is free space with $\epsilon_1 = \epsilon_0$, $\mu_1 = \mu_1$ and $\sigma_1 = 0$ so that $k_1 = k_0$.

The solution of the electromagnetic fields $\mathbf{E}_{mn}$ and $\mathbf{H}_{mn}$ of the wave modes mn can be found by using the well-known method of separation of variables. By assuming $E_{mn} = \psi_{mn}^e \hat{\phi}$ or $E_{mn} = \psi_{mn}^h \hat{\phi}$, the vector wave equations can be scalarized and the Helmholz scalar wave equations become separable.

The solutions of the wave equations are expressed in the following scalar wave functions for prolate spheroidal coordinates:

$$\psi_{mn}^{e,h} = S_{mn}(-ic, \eta) R_{mn}(-ic, i\xi) \begin{matrix}\cos \\ \sin\end{matrix} m\phi. \tag{3}$$

The angular and radial spheroidal functions, $S_{mn}(-ic, \eta)$ and $R_{mn}(-ic, i\xi)$, satisfy the ordinary differential equations given as follows [19, 20]:

$$\frac{d}{d\eta}\left[(1-\eta^2)\frac{d}{d\eta}S_{mn}(-ic,\eta)\right] + \left[\lambda_{mn} + c^2\eta^2 - \frac{m^2}{1-\eta^2}\right] S_{mn}(-ic,\eta) = 0, \tag{4a}$$

$$\frac{d}{d\xi}\left[(\xi^2+1)\frac{d}{d\xi}R_{mn}(-ic,i\xi)\right] - \left[\lambda_{mn} + c^2\xi^2 - \frac{m^2}{1-\xi^2}\right] R_{mn}(-ic,i\xi) = 0, \tag{4b}$$

where m and n identify the eigenvalue parameters. For the fields inside the spheroid, the first kind of radial function ($i = 1$) is taken;

and for the fields outside the spheroid, the third kind is used. For the intermediate region between the two spheroidal interfaces, both the first and third kind of the radial functions are used in the construction of the dyadic Green's functions, but this case will not be discussed here. The angular function is a function of the associate Legendre functions while the radial functions can be expressed as in terms of spherical Bessel functions.

3. ELECTROMAGNETIC FIELD REPRESENTATIONS

In this analysis, the incident, scattered, and transmitted wave fields ($\mathbf{E}^i$ & $\mathbf{H}^i$, $\mathbf{E}^s$ & $\mathbf{H}^s$, and $\mathbf{E}^t$ & $\mathbf{H}^t$) are expanded in terms of the spheroidal vector wave eigenfunctions $\mathbf{M}^{r(i)}_{\substack{e\\o}mn}$ and $\mathbf{N}^{r(i)}_{\substack{e\\o}mn}$. By matching the boundary conditions, the expansion coefficients of the series have been determined. Two types of polarized waves, i.e., the TE-mode (denoted as Case I) and TM-mode (denoted as Case II) excited waves, are considered.

3.1 Incident Wave Expressions in Rectangular Coordinates

Following the method described in [1, 3], the incident waves of parallel (I) and perpendicular (II) polarizations are given as follows:

$$\mathbf{E}^i_I = (\cos\alpha\hat{\mathbf{x}} - \sin\alpha\hat{\mathbf{z}})\exp[ik_0(x\sin\alpha + z\cos\alpha)], \tag{5a}$$

$$\mathbf{H}^i_I = \frac{k_0}{\omega\mu_0}\hat{\mathbf{y}}\exp[ik_0(x\sin\alpha + z\cos\alpha)]; \tag{5b}$$

and

$$\mathbf{E}^i_{II} = -\hat{\mathbf{y}}\exp[ik_0(x\sin\alpha + z\cos\alpha)], \tag{6a}$$

$$\mathbf{H}^i_{II} = \frac{k_0}{\omega\mu_0}(\cos\alpha\hat{\mathbf{x}} - \sin\alpha\hat{\mathbf{z}})\exp[ik_0(x\sin\alpha + z\cos\alpha)]. \tag{6b}$$

3.2 Expansions of Incident Fields Using Vector Eigenfunctions

For the ease of boundary matching, we expand the incident wave fields in terms of oblate spheroidal vector wave eigenfunctions. The expressions of the incident waves expanded are given below:

$$\begin{bmatrix} \mathbf{E}_I^i \\ \mathbf{H}_{II}^i \end{bmatrix} = \begin{bmatrix} 1 \\ \frac{-k_0}{\omega\mu_0} \end{bmatrix} \sum_{n=1}^{\infty} \sum_{m=0}^{n} i^n \Big[g_{mn}^i \mathbf{M}_{emn}^{r(1)}(k_0) + i f_{mn}^i \mathbf{N}_{omn}^{r(1)}(k_0) \Big], \quad (7a)$$

$$\begin{bmatrix} \mathbf{E}_{II}^i \\ \mathbf{H}_I^i \end{bmatrix} = \begin{bmatrix} 1 \\ \frac{k_0}{\omega\mu_0} \end{bmatrix} \sum_{n=1}^{\infty} \sum_{m=0}^{n} i^n \Big[f_{mn}^i \mathbf{M}_{omn}^{r(1)}(k_0) - i g_{mn}^i \mathbf{N}_{emn}^{r(1)}(k_0) \Big], \quad (7b)$$

where the oblate spheroidal vector wave eigenfunctions are given in terms of the scalar wave functions as follows:

$$\mathbf{M}_{\substack{e \\ o}mn}^{r(l)}(ka, \zeta) = \nabla \times \left[S_{mn}(-ic, \eta) R_{mn}^{(l)}(-ic, i\xi) \begin{matrix} \cos \\ \sin \end{matrix} m\phi \hat{\mathbf{r}} \right], \quad (8a)$$

$$\mathbf{N}_{\substack{e \\ o}mn}^{r(l)}(ka, \zeta) = \frac{1}{k} \nabla \times \nabla \times \left[S_{mn}(-ic, \eta) R_{mn}^{(l)}(-ic, i\xi) \begin{matrix} \cos \\ \sin \end{matrix} m\phi \hat{\mathbf{r}} \right]; \quad (8b)$$

and the expansion coefficients are expressed below:

$$f_{mn}^i = \frac{4m}{\sum_{r=0,1}^{\infty}{}' \frac{2(d_r^{mn})^2 (r+2m)!}{(2r+2m+1) r!}} \sum_{r=0,1}^{\infty}{}' \frac{d_r^{mn} P_{m+r}^m(\cos\alpha)/\sin\alpha}{(r+m)(r+m+1)}, \quad (9a)$$

$$g_{mn}^i = \frac{2(2-\delta_{m0})}{\sum_{r=0,1}^{\infty}{}' \frac{2(d_r^{mn})^2 (r+2m)!}{(2r+2m+1) r!}} \sum_{r=0,1}^{\infty}{}' \frac{d_r^{mn} P_{m+r}^m(\cos\alpha)/\sin\alpha}{(r+m)(r+m+1)}. \quad (9b)$$

In Eq. (9), $P_n^m(x)$ stands for the associated Legendre function, the coefficient d_r^{mn} is given in [19], and the prime over the summation sign indicates that the summation is carried out over only the even values of r when $n-m$ is even, and over only the odd values of r when $n-m$ is odd. Explicit forms of the oblate spheroidal vector wave functions are detailed in [19], and hence will not be presented here.

4. EXPANSION OF SCATTERED AND TRANSMITTING ELECTROMAGNETIC FIELDS

To determine the scattered and transmitting electromagnetic fields (in the outer and inner regions of the raindrop-divided oblate spheroidal structure, we use vector wave eigenfunction expansion to express them. In a form similar to the expanded incident wave fields, the scattered

electromagnetic fields ($\mathbf{E}^s$ and $\mathbf{H}^s$) for parallel (I) and perpendicular (II) polarizations are represented as follows:

$$\begin{bmatrix} \mathbf{E}_I^s \\ \mathbf{H}_{II}^s \end{bmatrix} = \begin{bmatrix} 1 \\ \frac{-k_0}{\omega\mu_0} \end{bmatrix} \sum_{n=1}^{\infty} \sum_{m=0}^{n} i^n \left[g_{mn}^{s_{II}^I} \mathbf{M}_{emn}^{r(1)}(k_0) + i f_{mn}^{s_{II}^I} \mathbf{N}_{omn}^{r(1)}(k_0) \right], \tag{10a}$$

$$\begin{bmatrix} \mathbf{E}_{II}^s \\ \mathbf{H}_I^s \end{bmatrix} = \begin{bmatrix} 1 \\ \frac{k_0}{\omega\mu_0} \end{bmatrix} \sum_{n=1}^{\infty} \sum_{m=0}^{n} i^n \left[f_{mn}^{s_I^{II}} \mathbf{M}_{omn}^{r(1)}(k_0) - i g_{mn}^{s_I^{II}} \mathbf{N}_{emn}^{r(1)}(k_0) \right]; \tag{10b}$$

while the transmitting fields ($\mathbf{E}^t$ and $\mathbf{H}^t$ are given below

$$\begin{bmatrix} \mathbf{E}_I^t \\ \mathbf{H}_{II}^t \end{bmatrix} = \begin{bmatrix} 1 \\ \frac{-k_0\sqrt{\epsilon_r}}{\omega\mu_0} \end{bmatrix} \sum_{n=1}^{\infty} \sum_{m=0}^{n} i^n \left[g_{mn}^{t_{II}^I} \mathbf{M}_{emn}^{r(1)}(k_0) + i f_{mn}^{t_{II}^I} \mathbf{N}_{omn}^{r(1)}(k_0) \right], \tag{11a}$$

$$\begin{bmatrix} \mathbf{E}_{II}^t \\ \mathbf{H}_I^t \end{bmatrix} = \begin{bmatrix} 1 \\ \frac{k_0\sqrt{\epsilon_r}}{\omega\mu_0} \end{bmatrix} \sum_{n=1}^{\infty} \sum_{m=0}^{n} i^n \left[f_{mn}^{t_I^{II}} \mathbf{M}_{omn}^{r(1)}(k_0) - i g_{mn}^{t_I^{II}} \mathbf{N}_{emn}^{r(1)}(k_0) \right]. \tag{11b}$$

It is seen that we have four sets of unknown coefficients ($f_{mn}^{s_I^{II}}$, $g_{mn}^{s_I^{II}}$, $f_{mn}^{t_I^{II}}$ and $g_{mn}^{t_I^{II}}$) to be determined.

4.1 Boundary Conditions at $\xi = \xi_0$ in Scalar Form

To determine the aforementioned four unknown coefficients, we need to apply the boundary conditions at $\xi = \xi_0$. In vector form, the boundary conditions can be expressed as follows:

$$\hat{\xi} \times \left\{ \begin{bmatrix} \mathbf{E}^{i}{}_{I} \\ {}_{II} \\ \mathbf{H}^{i}{}_{I} \\ {}_{II} \end{bmatrix} + \begin{bmatrix} \mathbf{E}^{s}{}_{I} \\ {}_{II} \\ \mathbf{H}^{s}{}_{I} \\ {}_{II} \end{bmatrix} \right\} = \hat{\xi} \times \begin{bmatrix} \mathbf{E}^{t}{}_{I} \\ {}_{II} \\ \mathbf{H}^{t}{}_{I} \\ {}_{II} \end{bmatrix}. \tag{12}$$

As mentioned earlier, both parallel and perpendicular polarizations are considered. To detail the tangential components of the electromagnetic fields on the surface $\xi = \xi_0$, the subsequent two subsections address the boundary conditions in the component form.

4.2 TE-Mode Excitation

For the parallel polarized waves (or TE-mode excitation), we express the boundary conditions in the explicit component form as follows (the term before the colon symbol specifies the *boundary condition for that component*):

$$
\begin{aligned}
E_\eta^I \quad : \quad & \sum_{n=m}^{\infty} i^n \Big[V_{mn}^{(3),t}(c_1) f_{mn}^{sI} + U_{mn}^{(3),t}(c_1) g_{mn}^{sI} \\
& \qquad - V_{mn}^{(3),t}(c_1) f_{mn}^{tI} + U_{mn}^{(3),t}(c_1) g_{mn}^{tI} \Big] \\
& = - \sum_{n=m}^{\infty} i^n V_{mn}^{(3),t}(c_1) f_{mn}^{i} + U_{mn}^{(3),t}(c_1) g_{mn}^{i}, \qquad (13a) \\
E_\phi^I \quad : \quad & \sum_{n=m}^{\infty} i^n \Big[Y_{mn}^{(3),t}(c_1) f_{mn}^{sI} + X_{mn}^{(3),t}(c_1) g_{mn}^{sI} \\
& \qquad - Y_{mn}^{(3),t}(c_1) f_{mn}^{tI} + X_{mn}^{(3),t}(c_1) g_{mn}^{tI} \Big] \\
& = - \sum_{n=m}^{\infty} i^n Y_{mn}^{(3),t}(c_1) f_{mn}^{i} + X_{mn}^{(3),t}(c_1) g_{mn}^{i}, \qquad (13b) \\
H_\eta^I \quad : \quad & \sum_{n=m}^{\infty} i^n \Big[U_{mn}^{(3),t}(c_1) f_{mn}^{sI} + V_{mn}^{(3),t}(c_1) g_{mn}^{sI} \\
& \qquad - \sqrt{\epsilon_r} U_{mn}^{(1),t}(c_2) f_{mn}^{tI} - \sqrt{\epsilon_r} V_{mn}^{(1),t}(c_2) g_{mn}^{tI} \Big] \\
& = - \sum_{n=m}^{\infty} i^n \Big[U_{mn}^{(1),t}(c_2) f_{mn}^{i} + V_{mn}^{(1),t}(c_2) g_{mn}^{i} \Big], \qquad (13c) \\
H_\phi^I \quad : \quad & \sum_{n=m}^{\infty} i^n \Big[X_{mn}^{(3),t}(c_1) f_{mn}^{sI} + Y_{mn}^{(3),t}(c_1) g_{mn}^{sI} \\
& \qquad - \sqrt{\epsilon_r} X_{mn}^{(1),t}(c_2) f_{mn}^{tI} - \sqrt{\epsilon_r} Y_{mn}^{(1),t}(c_2) g_{mn}^{tI} \Big] \\
& = - \sum_{n=m}^{\infty} i^n \Big[X_{mn}^{(1),t}(c_2) f_{mn}^{i} + Y_{mn}^{(1),t}(c_2) g_{mn}^{i} \Big], \qquad (13d) \\
& (m = 0, 1, 2, \cdots; \quad t = 0, 1, 2, \cdots)
\end{aligned}
$$

where $U_{mn}^{(1,3),t}(c_{1,2})$, $V_{mn}^{(1,3),t}(c_{1,2})$, $X_{mn}^{(1,3),t}(c_{1,2})$, and $Y_{mn}^{(1,3),t}(c_{1,2})$ are four known coefficients given in (A-1a)–(A-1d) and (A-2a)–(A-2c) in Appendix A.

4.3 TM-Mode Excitation

For the perpendicular polarized waves (or TM-mode excitation), similarly the boundary conditions are expressed in the component form below:

$$\begin{aligned} E_\eta^{II} \quad : \quad & \sum_{n=m}^{\infty} i^n \Big[U_{mn}^{(3),t}(c_1) f_{mn}^{sII} + V_{mn}^{(3),t}(c_1) g_{mn}^{sII} \\ & \qquad - U_{mn}^{(3),t}(c_1) f_{mn}^{tII} + V_{mn}^{(3),t}(c_1) g_{mn}^{tII} \Big] \\ & = - \sum_{n=m}^{\infty} i^n U_{mn}^{(3),t}(c_1) f_{mn}^{i} + V_{mn}^{(3),t}(c_1) g_{mn}^{i}, \qquad (14a) \\ E_\phi^{II} \quad : \quad & \sum_{n=m}^{\infty} i^n \Big[X_{mn}^{(3),t}(c_1) f_{mn}^{sII} + Y_{mn}^{(3),t}(c_1) g_{mn}^{sII} \\ & \qquad - X_{mn}^{(3),t}(c_1) f_{mn}^{tII} + Y_{mn}^{(3),t}(c_1) g_{mn}^{tII} \Big] \\ & = - \sum_{n=m}^{\infty} i^n X_{mn}^{(3),t}(c_1) f_{mn}^{i} + Y_{mn}^{(3),t}(c_1) g_{mn}^{i}, \qquad (14b) \\ H_\eta^{II} \quad : \quad & \sum_{n=m}^{\infty} i^n \Big[V_{mn}^{(3),t}(c_1) f_{mn}^{sII} + U_{mn}^{(3),t}(c_1) g_{mn}^{sII} \\ & \qquad - \sqrt{\epsilon_r} V_{mn}^{(1),t}(c_2) f_{mn}^{tII} - \sqrt{\epsilon_r} U_{mn}^{(1),t}(c_2) g_{mn}^{tII} \Big] \\ & = - \sum_{n=m}^{\infty} i^n \Big[V_{mn}^{(1),t}(c_2) f_{mn}^{i} + U_{mn}^{(1),t}(c_2) g_{mn}^{i} \Big], \qquad (14c) \\ H_\phi^{II} \quad : \quad & \sum_{n=m}^{\infty} i^n \Big[Y_{mn}^{(3),t}(c_1) f_{mn}^{sII} + X_{mn}^{(3),t}(c_1) g_{mn}^{sII} \\ & \qquad - \sqrt{\epsilon_r} Y_{mn}^{(1),t}(c_2) f_{mn}^{tII} - \sqrt{\epsilon_r} X_{mn}^{(1),t}(c_2) g_{mn}^{tII} \Big] \\ & = - \sum_{n=m}^{\infty} i^n \Big[Y_{mn}^{(1),t}(c_2) f_{mn}^{i} + X_{mn}^{(1),t}(c_2) g_{mn}^{i} \Big], \qquad (14d) \end{aligned}$$

where $U_{mn}^{(1,3),t}(c_{1,2})$, $V_{mn}^{(1,3),t}(c_{1,2})$, $X_{mn}^{(1,3),t}(c_{1,2})$, and $Y_{mn}^{(1,3),t}(c_{1,2})$ are the same known coefficients used in (13) and given in (A-1a)–(A-1d) and (A-2a)–(A-2c) in Appendix A.

The parameters $U_{mn}^{(j),t}$ and $V_{mn}^{(j),t}$ correspond to the $\hat{\eta}$-components of the vector wave functions $\mathbf{M}_{mn}^{r(j)}$ and $\mathbf{N}_{mn}^{r(j)}$ while the parameters $X_{mn}^{(j),t}$ and $Y_{mn}^{(j),t}$ correspond to the $\hat{\phi}$-components of the vector eigenfunctions, respectively. In the computation, the number t is taken as large as is needed to achieve the desired accuracy in the computation of the total cross sections.

5. EXTINCTION CROSS SECTION AND SPECIFIC RAINFALL ATTENUATION

5.1 Convergence Issues and Comparison of Results

As the analysis involves infinite series summations of the vector wave eigenfunctions, a detailed checking of the algorithm should be made to ensure that the program converges well and/or fast before the needed information is obtained. From the computations, it is found that truncation numbers depend upon (i) size of spheroids and (ii) orientation of the scatterers. In general, a small spheroid with a small ratio of a/b and a small refractive index requires a small value of convergence number, while a large spheroid with a large ratio of a/b and a large refractive index requires a large convergence number. The truncation condition used in [14] is also considered in the computation.

To examine and ensure the correctness of the program, the intensity function values of forward and backward scattered waves with parallel polarization incidence for prolate spheroids of various sizes have been computed and shown in Table 1. Also, these values are compared with the available data obtained by Asano and Yamamoto [13] in Table 1. It is seen clearly that the values obtained in this paper are in excellent agreement with the published data but are more accurate since more significant digits are provided.

5.2 Size Parameters of Raindrops

After the applicability of the algorithm is confirmed, we can start to compute the needed quantities. However, we have to set the oblate spheroidal raindrop parameters first. Therefore, the following equivolumic spherical raindrops are utilized [3]:

$$\frac{4}{3}\pi\bar{a}^3 = \frac{4}{3}\pi ab^2, \quad \text{and} \quad \frac{a}{b} = 1 - \bar{a}; \tag{15}$$

c	Forward Scattering		Backward Scattering	
	Asano and Yamamoto	calculated	Asano and Yamamoto	calculated
1	0.00646	0.00647753	0.00191	0.00191119
2	0.545	0.54507	0.00335	0.00334865
3	7.90	7.89861	0.0308	0.03075641
4	47.4	47.3682	0.268	—
5	163	163.293	1.07	—

Table 1. Comparison of intensity function values of forward and backward scattered waves at parallel polarization incidence for prolate spheroids of various sizes.

where a and b stand for the minor and major axes of the oblate spheroid and $\overline{a}$ (in cm) denotes the mean radius of the raindrops.

Furthermore, the basic parameters ξ_0 and d in oblate spheroidal coordinates can then be determined from the two equations given as follows:

$$a = \frac{d}{2}\xi_0, \tag{16a}$$

$$b = \frac{d}{2}(\xi_0^2 + 1)^{\frac{1}{2}}. \tag{16b}$$

Based on these relationships shown in Eq. (15) and Eq. (16), we have computed the needed parameters as showed in Table 2 to be used in the numerical analysis. Further, the coefficients c_1 and c_2 for various mean raindrop radius and operating frequencies are calculated and shown in Table 3 and Table 4.

It should be pointed out that in Singapore, three experimental links operating at 15 GHz, 21.225 GHz and 38 GHz have been established to collect the rain attenuation data. This is why we have chosen the three specific operating frequencies in the calculations. However, the parameters at other frequencies can also be obtained in the similar way as mentioned earlier.

5.3 Extinction (Total) Cross Section

After we have set the parameters for the computation, the total cross sections are computed shown below.

$\overline{a}$ (cm)	$\frac{a}{b} = 1 - \overline{a}$	ξ_0	d (cm)
0.025	0.975	4.38784	0.0112044
0.050	0.950	3.04243	0.0317635
0.075	0.925	2.43442	0.0584956
0.100	0.900	2.06474	0.0902941
0.125	0.875	1.80739	0.126540
0.150	0.850	1.61357	0.166832
0.175	0.825	1.45983	0.210895
0.200	0.800	1.33333	0.258532
0.225	0.775	1.22634	0.309601
0.250	0.750	1.13389	0.364003
0.275	0.725	1.05263	0.421675
0.300	0.700	0.98020	0.482518
0.325	0.675	0.91486	0.546715

Table 2. Spheroidal parameters ξ_0 and confocal distance d for various sizes of raindrops.

$\overline{a}$	Spheroidal size parameter c_1		
(cm)	(15 GHz)	(21.225 GHz)	(38 GHz)
0.025	0.0175998	0.0249038	0.0445862
0.050	0.0498938	0.0705999	0.126398
0.075	0.0918847	0.130017	0.232775
0.100	0.141834	0.200695	0.359312
0.125	0.198768	0.281257	0.503545
0.150	0.262059	0.370814	0.663884
0.175	0.331274	0.468752	0.839227
0.200	0.406101	0.574633	1.02879
0.225	0.486320	0.688143	1.23201
0.250	0.571775	0.809062	1.44850
0.275	0.662365	0.937247	1.67799
0.300	0.758037	1.07262	1.92036
0.325	0.858778	1.21517	2.17557

Table 3. The spheroidal size parameter c_1 of raindrop outer medium at various frequencies of incident waves.

$\overline{a}$	Spheroidal size parameter c_2		
(cm)	(15 GHz)	(21.225 GHz)	(38 GHz)
0.025	0.128289+i0.0449077	0.160958+i0.069982	0.223074+i0.122853
0.050	0.363687+i0.127309	0.456301+i0.198393	0.632394+i0.348277
0.075	0.669766+i0.234453	0.840325+i0.365361	1.16462 +i0.641387
0.100	1.03385 +i0.361903	1.29713 +i0.563972	1.79771 +i0.990048
0.125	1.44886 +i0.507176	1.81782 +i0.790360	2.51934 +i1.38747
0.150	1.91020 +i0.668671	2.39664 +i1.04203	3.32154 +i1.82927
0.175	2.41472 +i0.845278	3.02964 +i1.31724	4.19882 +i2.31241
0.200	2.96015 +i1.03621	3.71397 +i1.61478	5.14724 +i2.83473
0.225	3.54489 +i1.24089	4.44760 +i1.93375	6.16400 +i3.39468
0.250	4.16778 +i1.45894	5.22913 +i2.27355	7.24712 +i3.99119
0.275	4.82811 +i1.69009	6.05761 +i2.63376	8.39533 +i4.62354
0.300	5.52548 +i1.93421	6.93257 +i3.01418	9.60794 +i5.29136
0.325	6.25981 +i2.19126	7.85389 +i3.41476	10.8848 +i5.99457

Table 4. The spheroidal size parameter c_2 of raindrop inner medium at various frequencies of incident waves.

5.3.1 TE-Mode Excitation

For TE-excited wave illumination, the total (extinction) cross section is given below:

$$Q_{ext}^{I} = -\frac{\lambda^2}{\pi}\mathcal{R}e\sum_{n=1}^{\infty}\sum_{m=0}^{n}\left[\alpha_{1,mn}m\frac{S_{mn}(\cos\zeta)}{\sin\zeta} + \beta_{1,mn}\frac{dS_{mn}(\cos\zeta)}{d\zeta}\right], \tag{17a}$$

where $\lambda = \pi d/c^{(i)}$, different from the eigenvalue λ_{mn} in Eq. (4), stands for the wavelength in free space, and $\mathcal{R}e$ denotes the real part.

5.3.2 TM-Mode Excitation

Similarly, the total (extinction) cross section for TM-excited wave illumination is given by:

$$Q_{ext}^{II} = -\frac{\lambda^2}{\pi}\mathcal{R}e\sum_{n=1}^{\infty}\sum_{m=0}^{n}\left[\alpha_{2,mn}m\frac{S_{mn}(\cos\zeta)}{\sin\zeta} + \beta_{2,mn}\frac{dS_{mn}(\cos\zeta)}{d\zeta}\right]. \tag{17b}$$

5.3.3 Special Case: $\zeta = 0^\circ$

For parallel incidence, $\zeta = 0^\circ$, the total cross sections for both TE and TM modes reduce to

$$Q_{ext}^{I} = Q_{ext}^{II} = -\frac{\lambda^2}{\pi} \sum_{n=1}^{\infty} \left[\sum_{r=0,1}{}' \frac{(r+1)(r+2)}{2} d_r^{1n} \right] \mathcal{R}e[\alpha_{1n} + \beta_{1n}], \tag{17c}$$

where α_{1n} and β_{1n} are either $\alpha_{1,1n}$ and $\beta_{1,1n}$ or $\alpha_{2,1n}$ and $\beta_{2,1n}$, respectively, as these two sets are the same in this case.

Using the above formulas in Eq. (17) for both TE-mode and TM-mode excited waves, we have computed the total cross sections at the specific frequencies of 15 GHz, 21.225 GHz, and 38 GHz. The total cross sections calculated in this paper using the full-wave analysis and vector wave eigenfunction expansion are then compared with the data obtained using the T-Matrix Method in [21], as shown in Fig. 2. It is apparent that the two results obtained using different methods are very close with reasonably small errors. Although Asano and Yamamoto [13] had implemented the similar procedure in the calculation of scattering cross sections, they did not give any data of total cross sections.

5.3.4 Specific Rainfall Attenuation

After obtaining the total (extinction) cross sections $\overset{I}{Q}{}_{ext}^{II}$ for the TE-mode (I) or TM-mode (II) excitations, we can compute the specific attenuations using the following formula:

$$A_{\overset{I}{II}} = 4.343 \times 10^3 \int_0^{\infty} N(D) \overset{I}{Q}{}_{ext}^{II} dD, \qquad \text{dB/km}, \tag{18}$$

where $N(D)$ is the rain*d*rop *s*ize *d*istribution (DSD).

The randrop size distribution in Singapore's tropical environment has been obtained in 1993 by Yeo et al. [15] and then revised by Li et al. [16]. Following the similar procedure in [17, 18], we have obtained the specific attenuation at the three frequencies, 15 GHz, 21.225 GHz, and 38 GHz. The same procedure in [18] is followed to feed the total cross section data into Eq. (18). The TCS data obtained in this paper are found very close to those from the T-matrix approach [21] and the boundary point matching method [17]. The results of the specific

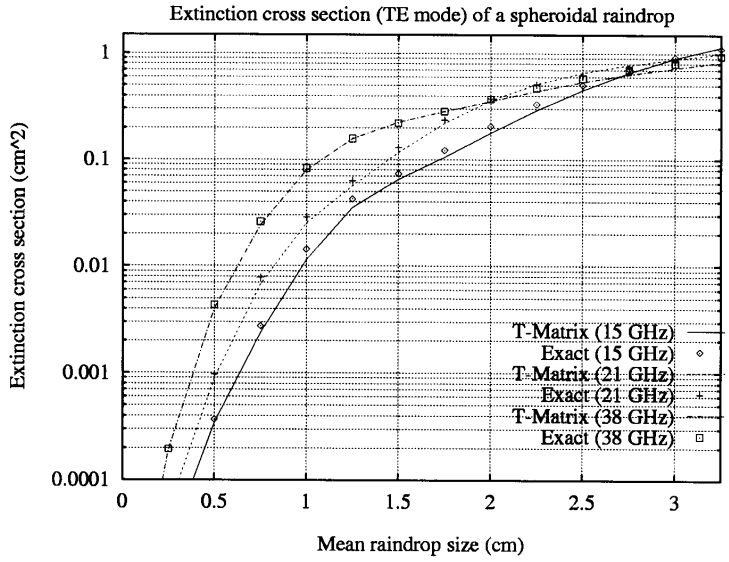

(a) TE-mode excitation.

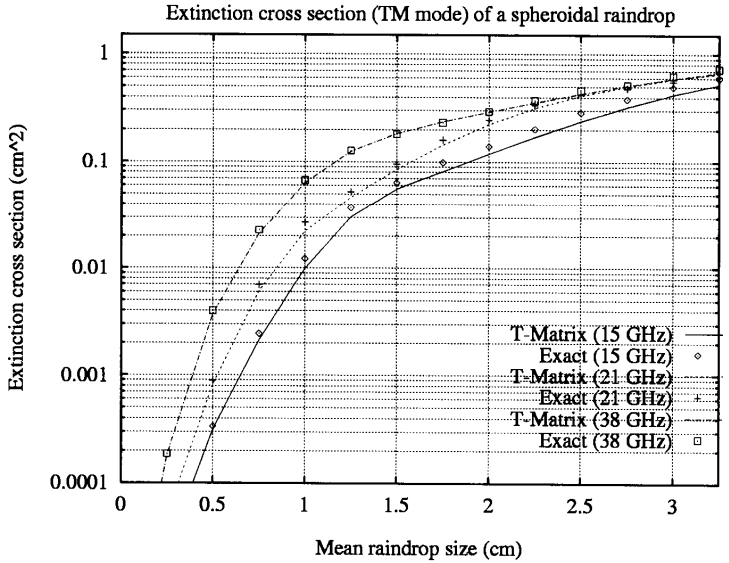

(b) TM-mode excitation.

Figure 2. Comparison between the results obtained from the exact spheroidal function analysis and the Waterman's T-matrix method.

attenuation obtained are also very close to those of [17]. To avoid repetition, this paper has not included the results of specific attenuation.

6. CONCLUSIONS

In this paper, electromagnetic wave scattering from the oblate spheroidal randrops of various sizes is studied using a full-wave technique that expands the incident waves, scattered waves, and transmitting waves into a series of oblate spheroidal vector wave eigenfunctions. The boundary conditions are then invoked to determine the scattering coefficients of the expanded fields. Exact and analytical results have been obtained in terms of the oblate radial and angular spheroidal harmonics. Both TE-mode and TM-mode incident plane waves are considered in the analysis. The raindrop is considered as a lossy medium having a permittivity which can be calculated using the Ray's fortran algorithm. As no commercial program exists so far for computing the oblate radial and angular spheroidal harmonics with complex arguments, an algorithm has been developed in this work under the software Mathematica ^{TM}. This algorithm is shown to be an accurate and efficient package by comparing the current results with the published data available in the public domain. Also, a comparison between the results obtained using the exact full-wave analysis and the T-matrix approach has been made and a very good agreement has been achieved.

APPENDIX A: INTERMEDIATE COEFFICIENTS $U_{mn}^{(j)t}(-ic)$, $V_{mn}^{(j)t}(-ic)$, $X_{mn}^{(j)t}(-ic)$, AND $Y_{mn}^{(j)t}(-ic)$

A The Coefficients for $m \geq 1$

In the case where $m \geq 1$, the intermediate coefficients, $U_{mn}^{(j)t}(-ic)$, $V_{mn}^{(j)t}(-ic)$, $X_{mn}^{(j)t}(-ic)$, and $Y_{mn}^{(j)t}(-ic)$, are expressed in closed form as follows:

$$\begin{aligned} U_{mn}^{(j)t}(-ic) =& m\xi_0 R_{mn}^{(j)}(-ic^{(h)}; i\xi_0) \\ & \times \Big[(\xi_0^2+1)^2 B_t^{mn}(-ic^{(h)}) - 2(\xi_0^2+1)^2 A_t^{mn}(-ic^{(h)}) \\ & + E_t^{mn}(-ic^{(h)}) \Big], \end{aligned} \tag{A-1a}$$

$$
\begin{aligned}
V_{mn}^{(j)t}(-ic) =& \frac{i}{c^{(h)}}\Bigg\{-\frac{m^2}{\xi_0^2+1}R_{mn}^{(j)}(-ic^{(h)};i\xi_0) \\
&\times\Big[(\xi_0^2+1)^2 D_t^{mn}(-ic^{(h)}) \\
&\quad -2(\xi_0^2+1)^2 C_t^{mn}(-ic^{(h)}) \\
&\quad +F_t^{mn}(-ic^{(h)})\Big]+R_{mn}^{(j)}(-ic^{(h)};i\xi_0) \\
&\times\left[\lambda_{mn}(-ic^{(h)})-(c^{(h)}\xi_0)^2-\frac{m^2}{\xi_0^2+1}\right] \\
&\times\Big[(\xi_0^2+1)C_t^{mn}(-ic^{(h)})-F_t^{mn}(-ic^{(h)})\Big] \\
&\quad +\xi_0(\xi_0^2+1)\left[\frac{dR_{mn}^{(j)}(-ic^{(h)};i\xi_0)}{d\xi_0}\right] \\
&\times\Big[-2C_t^{mn}(-ic^{(h)})+(\xi_0^2+1)G_t^{mn}(-ic^{(h)}) \\
&\quad -I_t^{mn}(-ic^{(h)})\Big]+R_{mn}^{(j)}(-ic^{(h)};i\xi_0) \\
&\times\Big[(\xi_0^2+1)^2 G_t^{mn}(-ic^{(h)}) \\
&\quad -(3\xi_0^2+1)I_t^{mn}(-ic^{(h)})\Big]\Bigg\}, \qquad \text{(A-1b)}
\end{aligned}
$$

$$
\begin{aligned}
X_{mn}^{(j)t}(-ic) =& \xi_0 R_{mn}^{(j)}(-ic^{(h)};i\xi_0)G_t^{mn}(-ic^{(h)}) \\
&+C_t^{mn}(-ic^{(h)})\left[\frac{dR_{mn}^{(j)}(-ic^{(h)};i\xi_0)}{d\xi_0}\right], \qquad \text{(A-1c)}
\end{aligned}
$$

$$
\begin{aligned}
Y_{mn}^{(j)t}(-ic) =& \frac{im}{c^{(h)}}\Bigg\{-(\xi_0^2+1)^{-1}R_{mn}^{(j)}(-ic^{(h)};i\xi_0) \\
&\times\Big[A_t^{mn}(-ic^{(h)})+H_t^{mn}(-ic^{(h)})\Big]+B_t^{mn}(-ic^{(h)}) \\
&\times\Big[R_{mn}^{(j)}(-ic^{(h)};i\xi_0) \\
&\quad +\xi_0\Big(\frac{dR_{mn}^{(j)}(-ic^{(h)};i\xi_0)}{d\xi_0}\Big)\Big]\Bigg\}, \qquad \text{(A-1d)}
\end{aligned}
$$

where $m=1,2,3,\cdots$ and $t=0,1,2,\cdots$.

B The Coefficients for $m=0$

In the case that $m=0$, the intermediate coefficients, $U_{0n}^{(j)t}(-ic)$,

$V_{0n}^{(j)t}(-ic)$, $X_{0n}^{(j)t}(-ic)$, and $Y_{0n}^{(j)t}(-ic)$, are further simplified and given as follows:

$$U_{0n}^{(j)t}(-ic) = Y_{(j)t}^{0n}(-ic) = 0, \tag{A-2a}$$

$$\begin{aligned} V_{0n}^{(j)t}(-ic) =& \frac{i}{c^{(h)}} \Bigg\{ + R_{0n}^{(j)}(-ic^{(h)}; i\xi_0) \left[\lambda_{0n} - \left(c^{(h)} \xi_0 \right)^2 \right] \\ & \left[\left(\xi_0^2 + 1 \right) C_t^{0n}(-ic^{(h)}) - F_t^{0n}(-ic^{(h)}) \right] \\ & + \xi_0 \left(\xi_0^2 + 1 \right) \left[\frac{dR_{0n}^{(j)}(-ic^{(h)}; i\xi_0)}{d\xi_0} \right] \\ & \times \left[-2C_t^{0n}(-ic^{(h)}) + \left(\xi_0^2 + 1 \right) G_t^{0n}(-ic^{(h)}) \right. \\ & \left. - I_t^{0n}(-ic^{(h)}) \right] + R_{0n}^{(j)}(-ic^{(h)}; i\xi_0) \\ & \left[\left(\xi_0^2 + 1 \right)^2 G_t^{0n}(-ic^{(h)}) \right. \\ & \left. - \left(3\xi_0^2 + 1 \right) I_t^{0n}(-ic^{(h)}) \right] \Bigg\}, \end{aligned} \tag{A-2b}$$

$$\begin{aligned} X_{0n}^{(j)t}(-ic) =& \xi_0 R_{0n}^{(j)}(-ic^{(h)}; i\xi_0) G_t^{0n}(-ic^{(h)}) \\ & + \left[\frac{dR_{0n}^{(j)}(-ic^{(h)}; i\xi_0)}{d\xi_0} \right] C_t^{0n}(-ic^{(h)}) \end{aligned} \tag{A-2c}$$

APPENDIX B: INTERMEDIATE COEFFICIENTS A_t^{mn} TO I_t^{mn}

A Special Relations Used in the Derivation

The following special relations are used in the derivation of the scattering coefficients.

The first is the normalized factor N_{mn} of the angular spheroidal functions $S_{mn}(ka, \cos\theta)$, given by:

$$N_{mn} = 2 \sum_{l=0,1}^{\infty}{}' \frac{(l+2m)!}{(2l+2m+1)l!} (d_l^{mn})^2. \tag{B-3}$$

The second and third relations used in the derivation are provided as follows:

$$\int_{-1}^{+1} P_\mu^m(\eta) P_\nu^m(\eta) d\eta = \frac{2}{2\mu+1} \frac{(\mu+m)!}{(\mu-m)!} \delta_{\mu\nu}, \tag{B-4a}$$

and

$$\int_{-1}^{+1} P_\mu^{m+2}(\eta) P_\nu^m(\eta) d\eta = \begin{cases} 0, & \nu > \mu; \\ -\frac{2}{2\mu+1} \frac{(\mu+m)!}{(\mu-m-2)!}, & \nu = \mu; \\ 2(m+1) \frac{(\mu+m)!}{(\mu-m-2)!}, & \nu < \mu. \end{cases} \tag{B-4b}$$

In addition, the following pair of equations is also used

$$\begin{aligned} &\frac{1}{(2m+2t-1)(2m+2t+1)} + \frac{1}{(2m+2t-3)(2m+2t-1)} \\ &\quad - \frac{2}{(2m+2t-3)(2m+2t+1)} = 0, \end{aligned} \tag{B-5a}$$

and

$$\begin{aligned} &\frac{(2m+t-2)}{(2m+2t-5)(2m+2t-3)(2m+2t-1)} \\ &- \frac{(4m+t-1)}{(2m+2t-5)(2m+2t-1)(2m+2t+1)} \\ &- \frac{(t-2m)}{(2m+2t-3)(2m+2t-1)(2m+2t+3)} \\ &+ \frac{(t+1)}{(2m+2t-1)(2m+2t+1)(2m+2t+3)} = 0. \end{aligned} \tag{B-5b}$$

For simplicity of the representation of the intermediates, the following two notations for the normalized coefficients $\mathcal{N}_1$ and $\mathcal{N}_2$ are assumed:

$$\mathcal{N}_1 = N_{m-1,m-1+t} = \frac{2}{2m+2t-1} \frac{(2m+t-2)!}{t!}, \tag{B-6a}$$

$$\mathcal{N}_2 = N_{1,1+t} = \frac{2}{2t+3} \frac{(t+2)!}{t!}. \tag{B-6b}$$

B The Coefficients for $m \geq 1$

In the case $m \geq 1$, the intermediates A_t^{mn} and I_t^{mn} are expressed in closed form as follows:

$$A_t^{mn} = [\mathcal{N}_1]^{-1} \sum_{r=0,1}{}' d_r^{mn} \int_{-1}^{+1} \eta(1-\eta^2)^{1/2} P_{m+r}^m(\eta) P_{m-1+t}^{m-1}(\eta) d\eta$$
$$= \frac{(2m+t)(2m+t-1)}{2m+2t+1} d_t^{mn} - \frac{t(t-1)}{2m+2t-3} d_{t-2}^{mn}, \tag{B-7a}$$
$$B_t^{mn} = [\mathcal{N}_1]^{-1} \sum_{r=0,1}{}' d_r^{mn} \int_{-1}^{+1} (1-\eta^2)^{-1/2} P_{m+r}^m(\eta) P_{m-1+t}^{m-1}(\eta) d\eta$$
$$= (2m+2t-1) \sum_{r=t}{}' d_r^{mn}, \tag{B-7b}$$
$$C_t^{mn} = [\mathcal{N}_1]^{-1} \sum_{r=0,1}{}' d_r^{mn} \int_{-1}^{+1} \eta(1-\eta^2)^{1/2} P_{m+r}^m(\eta) P_{m-1+t}^{m-1}(\eta) d\eta$$
$$= \frac{(2m+t-1)(2m+t)}{2m+2t+1} \left[\frac{2m+t+1}{2m+2t+3} d_{t+1}^{mn} + \frac{t}{2m+2t-1} d_{t-1}^{mn} \right]$$
$$- \frac{t(t-1)}{2m+2t-3} \left[\frac{2m+t-1}{2m+2t-1} d_{t-1}^{mn} + \frac{t-2}{2m+2t-5} d_{t-3}^{mn} \right], \tag{B-7c}$$
$$D_t^{mn} = [\mathcal{N}_1]^{-1} \sum_{r=0,1}{}' d_r^{mn} \int_{-1}^{+1} \eta(1-\eta^2)^{-1/2} P_{m+r}^m(\eta) P_{m-1+t}^{m-1}(\eta) d\eta$$
$$= t d_{t-1}^{mn} + (2m+2t-1) \sum_{r=t+1}{}' d_r^{mn}, \tag{B-7d}$$
$$E_t^{mn} = [\mathcal{N}_1]^{-1} \sum_{r=0,1}{}' d_r^{mn} \int_{-1}^{+1} (1-\eta^2)^{3/2} P_{m+r}^m(\eta) P_{m-1+t}^{m-1}(\eta) d\eta$$
$$= \frac{(2m+t-1)(2m+t)(2m+t+1)(2m+t+2)}{(2m+2t+1)(2m+2t+3)}$$
$$\cdot \left[\frac{d_t^{mn}}{(2m+2t+1)} - \frac{d_{t+2}^{mn}}{(2m+2t+5)} \right]$$
$$- \frac{2t(t-1)(2m+t)(2m+t-1)}{(2m+2t-3)(2m+2t+1)}$$
$$\cdot \left[\frac{d_{t-2}^{mn}}{(2m+2t-3)} - \frac{d_t^{mn}}{(2m+2t+1)} \right]$$
$$+ \frac{t(t-1)(t-2)(t-3)}{(2m+2t-5)(2m+2t-3)}$$
$$\cdot \left[\frac{d_{t-4}^{mn}}{(2m+2t-7)} - \frac{d_{t-2}^{mn}}{(2m+2t-3)} \right], \tag{B-7e}$$

$$
\begin{aligned}
F_t^{mn} &= [\mathcal{N}_1]^{-1} {\sum_{r=0,1}}' d_r^{mn} \int_{-1}^{+1} (1-\eta^2)^{3/2} P_{m+r}^m(\eta) P_{m-1+t}^{m-1}(\eta) d\eta \\
&= \frac{(2m+t-1)(2m+t)(2m+t+1)(2m+t+2)}{(2m+2t+1)(2m+2t+3)} \\
&\quad \cdot \frac{2m+t+3}{2m+2t+5} \left[\frac{d_{t+1}^{mn}}{2m+2t+3} - \frac{d_{t+3}^{mn}}{2m+2t+7} \right] \\
&\quad - \frac{t(t-2m)(2m+t-1)(2m+t)(2m+t+1)}{(2m+2t-3)(2m+2t+1)(2m+2t+3)} \\
&\quad \cdot \left[\frac{d_{t-1}^{mn}}{2m+2t-1} - \frac{d_{t+1}^{mn}}{2m+2t+3} \right] \\
&\quad - \frac{t(t-1)(t-2)(2m+t-1)(4m+t-1)}{2m+2t-5)(2m+2t-3)(2m+2t+1)} \\
&\quad \cdot \left[\frac{d_{t-3}^{mn}}{2m+2t-5} - \frac{d_{t-1}^{mn}}{2m+2t-1} \right] \\
&\quad + \frac{t(t-1)(t-2)(t-3)(t-4)}{(2m+2t-7)(2m+2t-5)(2m+2t-3)} \\
&\quad \cdot \left[\frac{d_{t-5}^{mn}}{2m+2t-9} - \frac{d_{t-3}^{mn}}{2m+2t-5} \right], \qquad \text{(B-7f)}
\end{aligned}
$$

$$
\begin{aligned}
G_t^{mn} &= [\mathcal{N}_1]^{-1} {\sum_{r=0,1}}' d_r^{mn} \int_{-1}^{+1} (1-\eta^2)^{1/2} \frac{dP_{m+r}^m(\eta)}{d\eta} P_{m-1+t}^{m-1}(\eta) d\eta \\
&= -t(m+t-1) d_{t-1}^{mn} + m(2m+2t-1) {\sum_{r=t-3}}' d_t^{mn}, \qquad \text{(B-7g)}
\end{aligned}
$$

$$
\begin{aligned}
H_t^{mn} &= [\mathcal{N}_1]^{-1} {\sum_{r=0,1}}' d_r^{mn} \int_{-1}^{+1} \eta (1-\eta^2)^{1/2} \frac{dP_{m+r}^m(\eta)}{d\eta} P_{m-1+t}^{m-1}(\eta) d\eta \\
&= -\frac{t(t-1)(m+t-2)}{2m+2t-3} d_{t-2}^{mn} - \frac{d_t^{mn}}{2(2m+2t+1)} \\
&\quad \cdot [t(t-1)(2m+2t+1) + (2m+t)(2m+t-1)] \\
&\quad + m(2m+2t-1) {\sum_{r=t+2}}' d_t^{mn}, \qquad \text{(B-7h)}
\end{aligned}
$$

$$
\begin{aligned}
I_t^{mn} &= [\mathcal{N}_1]^{-1} {\sum_{r=0,1}}' d_r^{mn} \int_{-1}^{+1} (1-\eta^2)^{3/2} \frac{dP_{m+r}^m(\eta)}{d\eta} P_{m-1+t}^{m-1}(\eta) d\eta \\
&= \frac{(m+t+2)(2m+t-1)(2m+t)(2m+t+1)}{(2m+2t+1)(2m+2t+3)} d_{t+1}^{mn}
\end{aligned}
$$

$$
\begin{aligned}
&- \left[\frac{t(2m+t-1)(2m+t)(m+t-1)}{(2m+2t-1)(2m+2t+1)} \right. \\
&\left. - \frac{t(t-1)(m+t)(2m+t-1)}{(2m+2t-3)(2m+2t-1)} \right] d_{t-1}^{mn} \\
&+ \frac{t(t-1)(t-2)(t+m-3)}{(2m+2t-5)(2m+2t-3)} d_{t-3}^{mn}. \qquad \text{(B-7i)}
\end{aligned}
$$

C The Coefficients for $m = 0$

In the case $m = 0$, the intermediates reduce to the following formulae:

$$
\begin{aligned}
C_t^{0n} &= [\mathcal{N}_1]^{-1} {\sum_{r=0,1}}' d_r^{0n} \int_{-1}^{+1} \eta (1-\eta^2)^{1/2} P_r^0(\eta) P_{1+t}^1(\eta) d\eta \\
&= \frac{1}{2t+1} \left[\frac{t+1}{2t+3} d_{t+1}^{0n} + \frac{t}{(2t-1)} d_{t-1}^{0n} \right] \\
&\quad - \frac{1}{2t+5} \left[\frac{t+3}{2t+7} d_{t+3}^{0n} + \frac{t+2}{(2t+3)} d_{t+1}^{0n} \right], \qquad \text{(B-8a)} \\
F_t^{0n} &= [\mathcal{N}_1]^{-1} {\sum_{r=0,1}}' d_r^{0n} \int_{-1}^{+1} \eta (1-\eta^2)^{3/2} P_r^0(\eta) P_{1+t}^1(\eta) d\eta \\
&= \frac{(t+3)(t+4)(t+5)}{(2t+5)(2t+7)} \\
&\quad \cdot \left[\frac{d_{1+t}^{0n}}{(2t+3)(2t+5)} - \frac{2 d_{t+3}^{0n}}{(2t+5)(2t+9)} \right. \\
&\qquad \left. + \frac{d_{t+5}^{0n}}{(2t+9)(2t+11)} \right] + \frac{3t(t+3)}{(2t+1)(2t+5)} \\
&\quad \cdot \left[\frac{d_{t-1}^{0n}}{(2t-1)(2t+1)} - \frac{2 d_{t+1}^{0n}}{(2t+1)(2t+5)} \right. \\
&\qquad \left. + \frac{d_{t+3}^{0n}}{(2t+5)(2t+7)} \right] - \frac{t(t-1)(t-2)}{(2t-1)(2t+1)} \\
&\quad \cdot \left[\frac{d_{t-3}^{0n}}{(2t-5)(2t-3)} - \frac{2 d_{t-1}^{0n}}{(2t-3)(2t+1)} \right. \\
&\qquad \left. + \frac{d_{t+1}^{0n}}{(2t+1)(2t+3)} \right], \qquad \text{(B-8b)}
\end{aligned}
$$

$$G_t^{0n} = [\mathcal{N}_1]^{-1} \sum_{r=0,1}{}' d_r^{0n} \int_{-1}^{+1} (1-\eta^2)^{1/2} \frac{dP_r^0(\eta)}{d\eta} P_{1+t}^1(\eta) d\eta$$
$$= d_{t+1}^{0n}, \tag{B-8c}$$

$$I_t^{0n} = [\mathcal{N}_1]^{-1} \sum_{r=0,1}{}' d_r^{0n} \int_{-1}^{+1} (1-\eta^2)^{3/2} \frac{dP_r^0(\eta)}{d\eta} P_{1+t}^1(\eta) d\eta$$
$$= \frac{1}{2t+1} \left[\frac{(t+1)(t+2)}{2t+3} d_{t+1}^{0n} - \frac{t(t-1)}{2t-1} d_{t-1}^{0n} \right]$$
$$- \frac{1}{2t+5} \left[\frac{(t+3)(t+4)}{2t+7} d_{t+3}^{0n} - \frac{(t+1)(t+2)}{2t+3} d_{t+1}^{0n} \right]. \tag{B-8d}$$

ACKNOWLEDGMENT

The authors wish to acknowledge Miss Chee-Luan Quek for her computational efforts. This work was supported in part by a grant under the NUS/Telecoms Joint R&D Project 018 and a grand under the MINDEF-NUS Joint R&D Project 13/96.

REFERENCES

1. Oguchi, T., "Attenuation of electromagnetic wave due to rain with distorted raindrops," *J. Radio Res. Labs.,* Vol. 7, 467–485, 1960.
2. Oguchi, T., "Attenuation of electromagnetic wave due to rain with distorted raindrops (Part II)," *J. Radio Res. Labs.,* Vol. 11, 19–44, 1964.
3. Morrison, J. A., and M. J. Cross, "Scattering of a plane electromagnetic wave by axisymmetric raindrops," *Bell Syst. Tech. J.,* Vol. 53, 955–1019, 1974.
4. Erma, V. A., "An exact solution for the scattering of electromagnetic waves from conductors of arbitrary shape: I. Case of cylindrical symmetry," *Phys. Rev.,* Vol. 173, 1243–1257, 1968.
5. Erma, V. A., "Exact Solution for the scattering of electromagnetic waves from conductors of arbitrary shape: II. General case," *Phys. Rev.,* Vol. 176, 1544–1553, 1968.
6. Erma, V. A., "Exact Solution for the scattering of electromagnetic waves from conductors of arbitrary shape: III. Obstacles with arbitrary electromagnetic properties," *Phys. Rev.,* Vol. 179, 1238–1246, 1969.

7. Holt, A. R., N. K. Uzunoglu, and B. G. Evans, "An integral equation solution to the scattering of electromagnetic radiation by dielectric spheroids and ellipsoids," *IEEE Trans. Antennas Propagat.,* Vol. AP-26, 706–712, 1978.
8. Waterman, P. C., "Matrix formulation of electromagnetic scattering," *Proc. IEEE,* Vol. 53, 805–812, 1965.
9. Waterman, P. C., "Scattering by dielectric obstacles," *Alta Freq.,* Vol. 38, 348–352, 1969.
10. Waterman, P. C, "Symmetry, unitarity, and geometry in electromagnetic scattering," *PHys. Review D,* Vol. 3, No. 4, 825–839, 1971.
11. Warner, C., "Effects of shape and orientation of spheroidal raindrops upon microwave scattering," *Electron. Lett.,* Vol. 11, 328–330, 1975.
12. Warner, C., and A. Hizal, "Scattering and depolarization of microwaves by spheroidal raindrops," *Radio Sci.,* Vol. 11, 921–930, 1976.
13. Asano, S., and G. Yamamoto, "Light scattering by a spheroidal particle," *Appl. Opt.,* Vol. 14, 29–49, 1975.
14. Cooray, M. F. R., and I. R. Ciric, "Electromagnetic wave scattering by a system of two spheroids of arbitrary orientation," *IEEE Trans. Antennas Propagat.,* Vol. AP-37, 608–618, 1989.
15. Yeo, T. S., P. S. Kooi, and M. S. Leong, "A two-year measurement of rainfall attenuation of CW microwaves in Singapore," *IEEE Trans. Antennas Propagat.,* Vol. AP-41, 709–712, 1993.
16. Li, L. W., T. S. Yeo, P. S. Kooi, and M. S. Leong, "Comment on raindrop size distribution model," *IEEE Trans. Antennas Propagat.,* Vol. 42, No. 9, 1360, September 1994.
17. Li, L. W., P. S. Kooi, M. S. Leong, T. S. Yeo, and M. Z. Gao, "Microwave attenuation by realistically distorted raindrops: Part I–Theory," *IEEE Trans. Antennas Propagat.,* Vol. 43, No. 8, 811–822, August 1995.
19. Li, L. W., P. S. Kooi, M. S. Leong, T. S. Yeo, and M. Z. Gao, "Microwave attenuation by realistically distorted raindrops: Part II–Predictions," *IEEE Trans. Antennas Propagat.,* Vol. 43, No. 8, 823–828, August 1995.
20. Stratton, J. A., P. M. Morse, L. J. Chu, J. D. C. Little, and F. J. Corbato, *Spheroidal wave functions,* John Wiley & Sons, New York, 1956.
21. Seow, Y. L., L. W. Li, M. S. Leong, P. S. Kooi, and T. S. Yeo, "An efficient TCS formula for rainfall microwave attenuation: T-matrix approach & 3-D fitting for oblate spheroidal raindrops," Submitted to *IEEE Trans. Antennas Propagat.,* June 1997.